This article has been accepted for publication in IEEE Transactions on NanoBioscience. This is the author's version which has not been fully edited and content may change prior to final publication. Citation information: DOI 10.1109/TNB.2022.3201237

Graphene-Based Metasurface Refractive Index Biosensor For Hemoglobin Detection: Machine Learning Assisted Optimization

Shobhit K. Patel, *Senior Member, IEEE*, Jaymit Surve, *Graduate Student Member, IEEE*, Juveriya Parmar, *Graduate Student Member, IEEE*, *Ayyanar Natesan* and Vijay Katkar, *Member, IEEE*

***Abstract*— Machine learning is the latest approach to optimize the performance of absorbers, sensors, etc. A sensor with behavior prediction using polynomial regression is presented. Three different variations of metasurfaces namely double split-ring resonator, single split ring resonator, split ring resonator with thin wire are analyzed. The proposed design aims to achieve the highest sensitivity by observing different designs and different parameter variation. The highest sensitivity is achieved for double split-ring resonator and single split ring resonator designs. The change in thickness of different parameter affect the absorption and the highest sensitivity is calculated based on these variations. The polynomial regression (PR) model is employed to predict the absorption values for assorted combinations of intermediate wavelength values with angle variation, substrate thickness, substrate length, substrate width, graphene potential, and resonator thickness values. Test Cases R-30 and R-50 are evaluated using R^2 score metric to assess the effectiveness of PR model for predicting the values of absorption. R^2 score close to 1.0 is achieved for all the experiments at a higher (more than 5) polynomial degree, which proves the prediction efficiency of a regression model. The proposed biosensor designed with a PR model can be applied in biomedical applications for hemoglobin detection.**

***Index Terms*—Graphene, Machine Learning, Metasurface, Polynomial Regression, Sensor**

This work was supported by Science and Engineering Research Board (SERB)-ASEAN-India Science and Technology Development Fund (AISTDF) under Grant IMRC/AISTDF/CRD/2018/000012.

Shobhit K Patel is with the Department of Computer Engineering, Marwadi University, Rajkot-360003, Gujarat, India (email: shobhitkumar.patel@marwadieducation.edu.in).

Jaymit Surve is with the Department of Electrical Engineering, Marwadi University, Rajkot-360003, Gujarat, India (email: jaymit.surve@marwadieducation.edu.in).

Juveriya Parmar is with the Department of Mechanical & Materials Engineering, University of Nebraska - Lincoln, 1400 R St., Lincoln, Nebraska 68588, USA (juveriyaparmar2@gmail.com). She was with the Department of Electronics and Communication Engineering, Marwadi University, Rajkot-360003, Gujarat, India

Ayyanar Natesan is with Department of Electronics and Communication Engineering, Thiagarajar College of Engineering, Madurai-620 015, Tamilnadu, India. (Email: naece@tce.edu)

Vijay Katkar is with the Department of Computer Engineering, Marwadi University, Rajkot-360003, Guajrat, India (email: vijay.katkar@mawadieducation.edu.in).

(Corresponding author: Ayyanar Natesan and Shobhit K. Patel)

I. INTRODUCTION

OPTICAL biosensors are the need in today's era because of their accurate detection of biomolecules which lead to their multiple applications in the field of medical, defense, environment, etc. [1]–[3]. Sensors are applicable in wearable sensing devices because of fast sensing [4]–[6]. The materials used for the biosensors are divided into three groups depending on their mechanism such as biocatalytic contains enzymes, affinity contains antibodies, and microbe containing organisms [1]. Biosensors are classified as electrochemical, thermometric, piezoelectric, optical, magnetic, etc and among them, optical sensors are mostly used [7]. Among the different properties of optical biosensors, refractive index sensing is mostly used because of its high absorption and sensitivity. An optical sensor changes its wavelength due to the binding of molecules that change the refractive index. The six major classifications of refractive index optical sensors are categorized as dielectric-based, metal-based, hybrid advanced based, SPR (surface plasmon resonance)-based, etc. SPR-based sensor aims at achieving good sensitivity due to its optical modes [8]. SPR biosensors are also classified into two categories labeled and label-free. Label-free overcomes the long procedure done by labeled biosensors [9].

Graphene is a monolayer sheet of graphite having excellent thermal properties, electric properties, and optical properties. These properties make it extraordinary from other materials [10][11]. Graphene mainly finds its application in sensor, and biomedical engineering, due to its excellent optical properties [12]. Graphene is easily combined with other nanomaterials which makes it more suitable for the fabrication of sensors and biosensors. When graphene is combined with metasurfaces then the sensitivity of the sensors is increased [13]. The graphene-based biosensor can also help in determining an iron deficiency in patients that suffer from anemia and this sensing help them in saving their lives from more dangerous diseases.[14]. Sensor-based on metamaterials is a great platform for terahertz applications. They can also be used for analyzing DNA structure [15].

A metamaterial is an artificially designed material due to its tremendous electromagnetic properties. They are artificially designed materials with desired properties such as optical properties, electrical properties, magnetic properties, etc [16]. The properties such as negative permittivity and negative permeability used in the material give the negative refractive

This article has been accepted for publication in IEEE Transactions on NanoBioscience. This is the author's version which has not been fully edited and content may change prior to final publication. Citation information: DOI 10.1109/TNB.2022.3201237

index [17]. Metamaterials are used due to their benefits such as compact size, cost-free, etc. They are also used in applications such as thermophotovoltaics, sensors, wireless communication, etc because of these benefits [18][19]. The advancement in nanofabrication technologies has led to great research interest and overcome many difficulties in the field of photonic metamaterials. They have progressed a lot due to their optical properties. They can be operated in any range of wavelengths from ultraviolet radiation to infrared radiation. It easily deals with light-matter interaction particles which helps in developing photonic devices. The properties of these sensing materials can be easily controlled by changing the geometrical parameters [20]-[21]. Pakarzadeh et al. presented a graphene-based photonic crystal sensor employing a D-shape with a 7500 nm/RIU sensitivity [22]. Askari and co-authors presented a terahertz sensor with a figure of merit of 19.44 RIU^{-1} for the detection of crystalline sugar [23]. Parizi et al. conveyed terahertz sensor based on graphene array for 1 to 8 THz with triple band absorption response and results verified the sensitivity towards the refractive index of coating layer [24]. Machine learning is used in many photonics structures for applications like absorbers, biosensors, etc [25]–[27]. Using Grid Search or Brute Force search to evaluate the entire set of tuning parameters for biosensor design requires a significant amount of computing power and time. Using a machine learning model trained on partially simulated data, the remaining design simulation parameters and values can be predicted. This can help to reduce the time and resources needed for the simulation.

The sensors designed so far are mainly worked on increasing their sensitivity by changing different parameters. We have proposed a machine learning algorithm to predict the values of absorption with different parameters. Three different cases are used for applying the machine learning approach to different parameters. The sensitivity is also observed and compared with other published results. The design, results, and conclusions are discussed in sections II to section IV respectively.

II. Design and Modeling

We have designed the graphene-based biosensor using COMSOL Multiphysics 6.0. The three different designs of metasurfaces are analyzed Design is analyzed with different geometrical parameters to achieve good sensitivity. The results are calculated in terms of absorption, electric field, and machine learning prediction values. The electric field plots are derived at a particular refractive index where the highest efficiency is achieved. The geometrical parameters such as graphene potential, angle variation, etc. are varied and response is observed. The meshing condition used in the design is tetrahedral which divides each corner and good results are derived. The hemoglobin is determined for separate concentrations of 10 g/l to 40 g/l with a uniform rise of 10 g/l and their particular refractive index ranging from 1.34, 1.36, 1.39, and 1.43 [28]. The resonator is made up of gold material. A graphene sheet is used for good electrical conductivity and helps in increased sensitivity. Silicon dioxide (SiO_2) material is used in the substrate. A graphene monolayer sheet is placed above the substrate and below the resonator. The primary reason for using gold is its improved features that contribute to the high efficiency of solar radiation absorption. There is a lot of information about gold's qualities in [29]. The procedure to avoid oxidation in gold metamaterials can be found in detail in ref. [30].

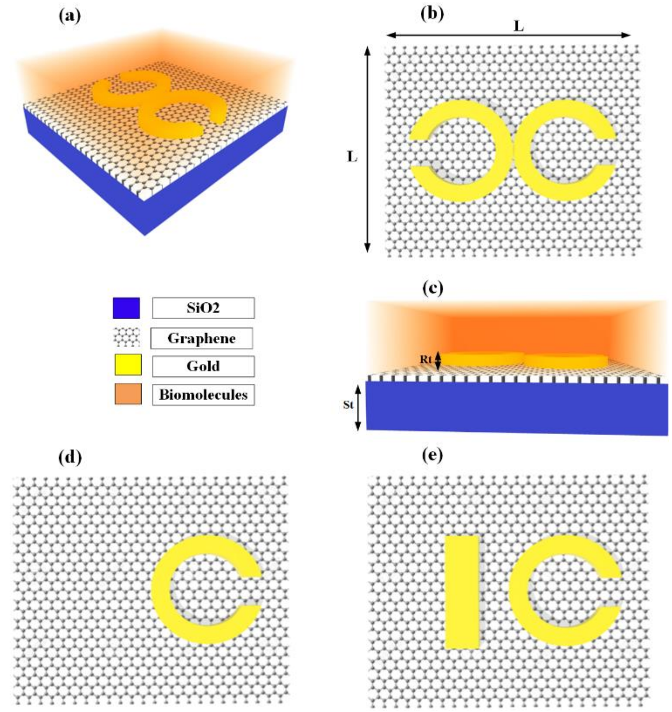

Fig. 1 GSRR biosensor design. (a) 3D view of GDSRR (b) Top view of GDSRR (c) Side view of GDSRR (d) Top view of the design (GSSRR) and (e) Top view of GSSRRTW

The schematic with different views for all three designs is presented in Fig. 1. Fig 1(a-c) has a 3d view of the side view of the GDSRR design. Fig. 1(d-e) is the top view of the graphene-based single split ring resonator (GSSRR) design and graphene-based single split ring resonator with thin wire (GSRRTW) design respectively. The thickness of the resonator (Rt) is 0.2 µm. The substrate thickness (St) is 0.6 µm. The length (L) and width (L) of the substrate are 70×70 μm^2. The detailed structural view is presented in Fig. 1. The color to the right indicates the materials used. We've created a refractive index sensor based on a metasurface here. The operational wavelength, lambda, must be smaller than or equal to lambda/4 in any metasurface structure. All sensors can be designed in the same way.

The sensitivity and other parameters are calculated as shown in Eq. (1) [28].

$$S = \frac{\Delta\lambda}{\Delta n} \tag{1}$$

$$FOM = \frac{S}{FWHM} \tag{2}$$

$$Q = \frac{\lambda_r}{FWHM} \tag{3}$$

$$DL = \left(\frac{\Delta n}{1.5}\right)\left(\frac{FWHM}{\Delta\lambda}\right)^{1.25} \tag{4}$$

This article has been accepted for publication in IEEE Transactions on NanoBioscience. This is the author's version which has not been fully edited and content may change prior to final publication. Citation information: DOI 10.1109/TNB.2022.3201237

III. Results and Discussion

The biosensor module accessible in Fig. 1 is simulated with the help of COMSOL Multiphysics and the results are analyzed in Fig. (2-6). The machine learning prediction results for three different models are presented in Fig. (7-14). Periodic boundary conditions are given to the design to maintain the periodicity of the design. The plots are defined for the concentration of hemoglobin for different refractive indexes. It is also defined for geometrical parameters of design. The machine learning approach is also detailed at the last of this section. The highest sensitivity is calculated for the proposed biosensor.

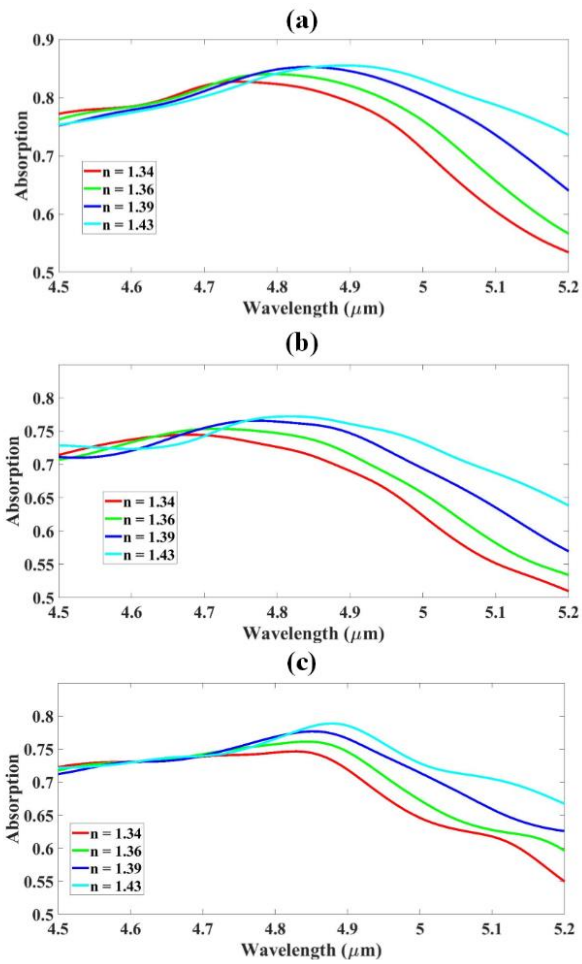

Fig. 2 Absorption response for different hemoglobin concentrations with refractive indices 1.34, 1.36, 1.39, and 1.43. It is simulated from the wavelength range of 4.5 μm to 5.2 μm. (a) GDSRR design (b) GSSRR design (c) GSSRRTW design

The absorption plots are derived in Fig 2 for three different metasurface designs. Fig. 2 (a-c) depicts the variation in absorption results as the refractive indices rise from 1.34 to 1.43 for GDSRR, GSSRR, and GSSRRTW designs. From Fig. 2 (a) GDSRR design's absorption response it is clear that the result moves towards the right as the RI increases. This phenomenon can also be observed in Fig. 2 (b-c) for the rest of the designs. The wavelength shift and its difference observed in the plot help in calculating the sensitivity that is clearly shown in the plot. The sensitivity for all the four different concentrations of the biomolecules is calculated and their comparison is presented in Table 1 for all three metasurface designs. The sensitivity of 2000 nm/RIU is for the first two concentrations of hemoglobin biomolecules for GDSRR design and GSSRR design. The GSSRRTW design has the largest sensitivity of 750 nm/RIU as shown in Table 1.

In Fig. 3(a), the line plot for the substrate thickness is given for absorption values. It is observed between 4.5 μm to 5.2 μm. The plot is defined at different points of the substrate thicknesses such as 0.6 μm, 0.7 μm, 0.8 μm, 0.9 μm,1μm, and 1.1μm. The highest efficiency of 85% is obtained at 1.1 μm substrate thickness. The rise in the substrate thickness helps in the overall absorption of the structure as it absorbs most of the light and minimum lights transmit through the substrate.

In Fig. 3(b), the line plot for the substrate width variation is given. It is observed between 4.5 μm to 5.2 μm. The range for the different values is designed and simulated at 70 μm to 75 μm with a gap of 1 μm plot. The range is fixed for the design and its geometrical parameters. The highest absorption for substrate depth can be observed at 84% for a value of 70 μm to 72 μm. The result is almost the same for all the values at the common refractive index. In Fig. 3(c), the line plot for the angle variation is observed. The angle is varied from 0° to 80° at a gap of 10°. The angle variation can be seen from the simulated range of 4.6 μm to 4.9 μm. The highest efficiency of 84% at 4.8 μm. The highest response is obtained from 60° to 80° for the angle variation parameter that can be observed from the color plot. The minimum absorption is obtained at 30°. The highest absorption is obtained at 0°.

TABLE 1
SENSITIVITY CALCULATION FOR CONCENTRATIONS HAVING REFRACTIVE INDICES 1.34, 1.36, 1.39, AND 1.43 FOR THREE DIFFERENT DESIGNS.

Design Parameters					
	n	**n_1** 1.34	**n_2** 1.36	**n_3** 1.39	**n_4** 1.43
Δn		0.02	0.03	0.04	
Double split ring resonator design	**λ (μm)**	4.75	4.79	4.84	4.89
	Δλ (nm)	40	50	50	
	S = Δλ/Δn	2000	1666	1250	
Single split ring resonator design	**λ (μm)**	4.68	4.72	4.77	4.82
	Δλ (nm)	40	50	50	
	S = Δλ/Δn	2000	1666	1250	
Single split ring resonator and thin wire design	**λ (μm)**	4.83	4.84	4.85	4.88
	Δλ (nm)	10	10	30	
	S = Δλ/Δn	500	333	750	

In Fig. S1(a-b), the line plot and color plot for the graphene chemical potential are observed. The plot is defined from values such as 0.1 eV to 0.9 eV with 0.1 eV gap. There is not much change in absorption. In Fig. S1(c-d), the line plot and color plot for the resonator thickness are observed. the plot is defined from values such as 0.2 μm to 0.5 μm with a 0.1 μm gap. The highest efficiency of 85% is obtained. The plot of permittivity, refractive index, permeability, conductivity, and impedance is presented in Fig. S2. The results are presented for both imaginary and real parts of the value. The results presented in the figures clearly show that the design is showing metamaterial behavior and has negative permittivity, permeability, and refractive index value for a certain wavelength range. The electric field results of the proposed design are available in Fig. 4 for three wavelengths 4.9 µm, 4.6 µm, and 5 µm. The higher absorption is visible at around 4.9 µm which is also similar to the absorption results available in Fig. 2. And as we can observe in Fig. 4 that for all the wavelengths the electric field distribution is almost the same and most of the electric field is concentrated around the double c structure and these much amount of electric field validates the high absorption response of the proposed GDSRRR structure.

Figure S3 in the supplemental materials shows that the linear fitting equation's R^2 of 0.9895 ensures linear sensing and reproducibility of the results. The developed biosensor design is equated with available designs from references [34-41] and a comparison is made available in Table 2. Sputtering, lithography, and the most recent printing techniques can all be used to make biosensors, but other well-known production methods include electrodeposition, electrochemical exfoliation, and electrospinning [31].

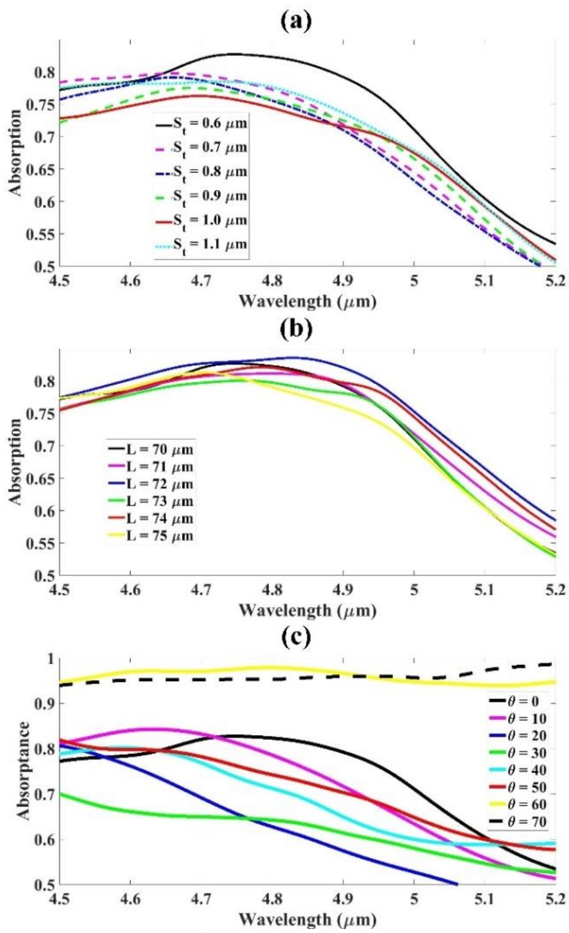

Fig. 3 Absorptance plots for numerous parameter variations. a) Line plot for substrate thickness change from 0.6 µm to 1.1 µm. b) Line plot for substrate width variation from 70 µm to 75 µm. c) Line plot for an angle of incidence variation from 0° to 80°.

The structure with a narrowband response and high Q absorbers is indeed the best choice for sensing applications. Though here we are achieving a high sensitivity to detect the hemoglobin biomolecules and the higher sensitivity is highly needed to distinguish the different concentrations of hemoglobin. Hence the biggest advantage of the proposed refractive index sensor is its sensitivity. Furthermore, nowadays researchers are focusing on low FOM structures and we are clearly achieving the lowest figure of merit for the proposed structure. That is the 2nd advantage of the proposed structure.

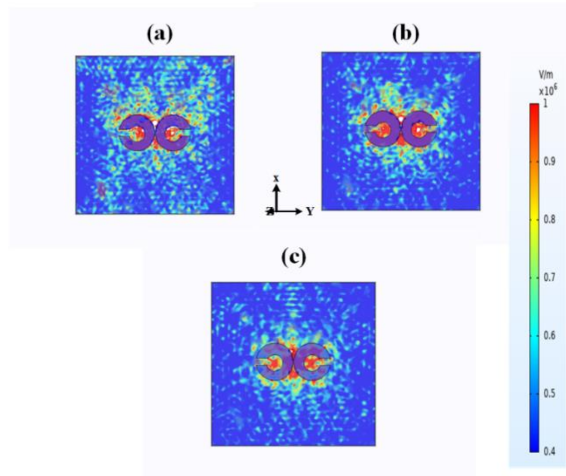

Fig. 4 Electric field results for three wavelengths of double split-ring resonator design (a) 4.9 µm (b) 4.6 µm (c) 5µm. The results are having better absorption around 4.9 µm wavelength range.

TABLE 2
SENSITIVITY ASSESSMENT OF DIFFERENT PUBLISHED DESIGNS WITH PROPOSED BIOSENSOR DESIGN

Biosensor design	Sensitivity	FOM (RIU^{-1})	Q Factor	Application
Ref. [32]	361.3 nm/RIU	-	1143	Hemoglobin detection
Ref. [33]	387.48 nm/RIU	-	-	Biosensing
Ref [34]	150 GHz/RIU	10.54	3.85	Hemoglobin detection, Encoding
Ref. [35]	0.243 THz/RIU	3.3	14.2	Polarization direction sensing
Ref [36]	1.421 µm/RIU	-	-	Hemoglobin Detection
Ref [37]	294 nm/RIU	-	-	-
Ref [38]	929 nm/RIU	-	-	-
Ref [39]	700 nm/RIU	-	-	Sensing
Ref [40]	1139 nm/RIU	-	-	Sensing
Proposed GDSRR design	2000 nm/RIU	0.54	1.29	Hemoglobin Detection
Proposed GSSRR design	2000 nm/RIU	0.5	1.24	Hemoglobin Detection
Proposed GSSRRTW design	750 nm/RIU	0.43	1.17	Hemoglobin Detection

IV. BEHAVIOR PREDICTION USING POLYNOMIAL REGRESSION

Experiments are designed and performed to discover if Polynomial Regression (PR) model can be employed to predict the values of absorption for in-between/intermediate wavelength in assorted cases. The basic fact used for experimentation is, that iff two variables are correlated, then in order to predict the value of one variable based on the value of

This article has been accepted for publication in IEEE Transactions on NanoBioscience. This is the author's version which has not been fully edited and content may change prior to final publication. Citation information: DOI 10.1109/TNB.2022.3201237

another, regression analysis or statistical methods might be used.

Correlation analysis is the most widely used approach to discover the existence of a relationship between two variables. Equation (5) is used to calculate joint changeability (Covariance) among two variables [41].

$$\mathrm{Cov(X,Y)} = \frac{\sum_{i=i}^{N}(x_i - \bar{X}) * (y_i - \bar{Y})}{N} \quad (5)$$

Since Covariance is not normalized, it is not easy to interpret the value of covariance. Pearson's Correlation coefficient (ρ) is a normalized Covariance value computed using equation (6).

$$\rho(\mathrm{X,Y}) = \frac{\mathrm{Cov(X,Y)}}{\sigma X * \sigma Y} \quad (6)$$

Pearson's Correlation (PC) measures whether two variables are linearly related. A positive score implies a positive linear correlation, whereas a negative value suggests a negative linear correlation. Zero means there exists no linear relationship between two variables.

The presence of non-linear correlation is verified using Spearman's Correlation (SC) coefficient and it is computed using equation (7).

$$\rho\mathrm{R(X),R(Y)} = \frac{\mathrm{Cov(R(X),R(Y))}}{\sigma R(X) * \sigma R(Y)} \quad (7)$$

Covariance, PC, SC between wavelength and various Angles, Graphene Potential, Resonator thickness, Substrate length, Substrate thickness, and Substrate width values are illustrated by means of the heat map table in supplementary Fig. S4 (a-f). It can be easily concluded from these results that, there exists a non-linear correlation between wavelength and remaining values. To model, this non-linear relation PR models with 3 and higher polynomial degrees are used.

Regression Analysis (RA) represents the association among dependent and independent variable(s) using equation (8). Here; i[th] dependent variable value is y_i, i[th] independent variable value is xi and the remaining terms are constants [42].

$$y_i = \beta_0 + \beta_1 x_i \quad (8)$$

PR is a different circumstance of RA that uses equation (9) to represent the association among dependent and independent variable(s).

$$y_i = \beta_0 + \beta_1 x_i^1 + \beta_2 x_i^2 + \beta_3 x_i^3 + \cdots + \beta_m x_i^m \quad (9)$$

Test Case (TC) R-30 and TC R-50 are used to measure the prediction proficiency of PR models. In TC R-M, two non-overlapping subsets of randomly selected M% and (100-M)% records from simulated data are created. A subset with (100-M)% records is used to train the polynomial regression model whereas a subset with M% records is utilized to test its prediction proficiency.

In these experiments, the wavelength is used as a dependent variable, and PR is utilized to predict absorption value. The Metric used to determine the efficiency of prediction models is the R^2 score. Equation (10) is used to calculate the R^2 score.

$$R^2 = 1 - \frac{\sum_1^N(Predicted\ TargetValue_i - ActualTargetV\ldots}{\sum_{i=1}^N(ActualTarget_i - \ Average\ TargetValu\ldots} \quad (10)$$

The effectiveness of models trained using numerous combinations of angle and polynomial degree values is shown in Fig. 5(a) for TC R-30 and 5(b) for TC R-50 with the help of a heat map table representing R^2 Score. Fig. 5 illustrates that R^2 score of 1.0 can be obtained for angles 0◦ to 50◦ and 800 at polynomial degrees 4, 5, and 6. For angle 60◦ and 70◦ R^2 score of 0.98, 0.97 is obtained respectively at polynomial degree 7.

The effectiveness of models trained using numerous combinations of graphene potential and polynomial degree values is shown in Fig. 6 (a) for TC R-30 and 6 (b) for TC R-50 with the help of the heat map table (HMT) representing R^2 score. Fig. 6 illustrates that R^2 score of 1.0 can be obtained for all graphene potential values at polynomial degrees 4, 5, and 6.

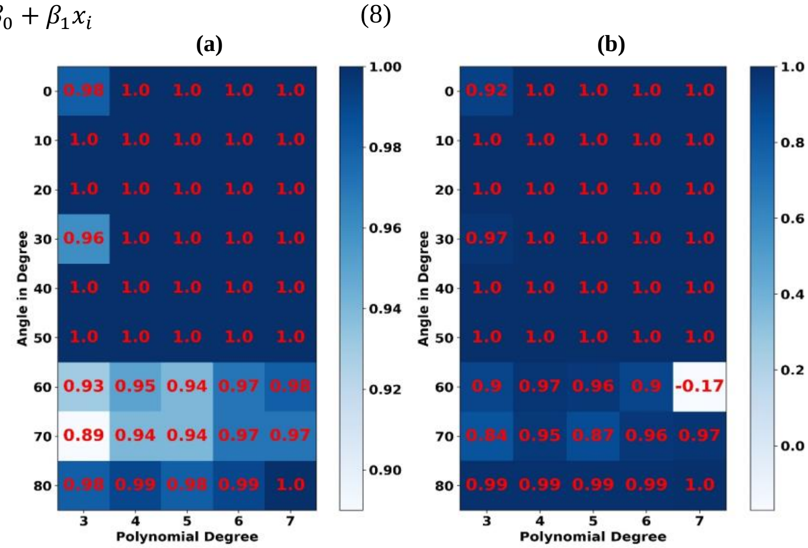

Fig. 5 HMT indicating R^2 Score of PR models using numerous combinations of angle with polynomial degrees for (a) TCR-30 (b) TCR-50

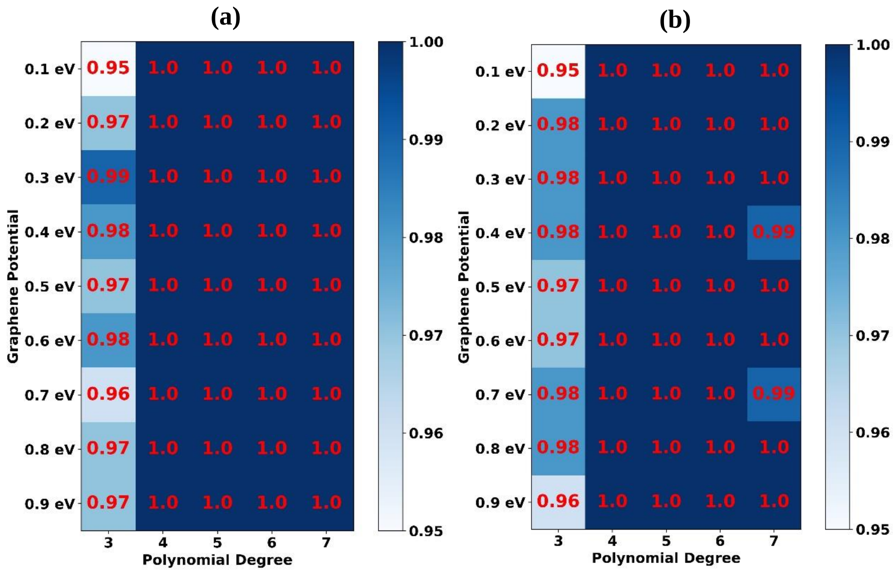

Fig. 6 HMT indicating R^2 Score of PR models using numerous combinations of graphene potential with polynomial degrees for (a) TCR-30 (b) TCR-50

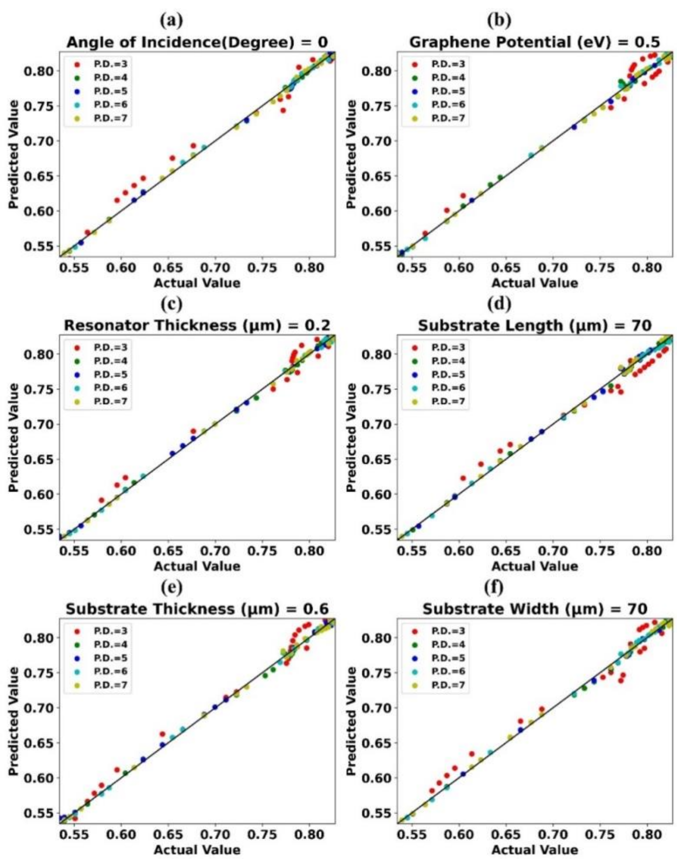

Fig.7 Values of absorption predicted by PR model vs Simulated values of absorption for test Case R-30 and (a) Angle = 0 (b) Graphene Potential = 0.5 eV (c) Resonator Thickness = 0.2 µm (d) Substrate Length = 70 µm (e) Substrate Thickness = 0.6 µm (f) Substrate Width = 70 µm.

The effectiveness of models trained using numerous combinations of resonator thickness and polynomial degree values is shown in Fig. S5(a) for TC R-30 and S5(b) for TC R-50 with the help of a heat map table representing R^2 score. Fig. S5 illustrates that R^2 score of 1.0 can be obtained for all resonator thickness values at polynomial degrees 4 and higher.

The effectiveness of models trained using numerous combinations of substrate length and polynomial degree values is shown in Fig. S6(a) for TC R-30 and S6(b) for TC R-50 with the help of a heat map table representing R^2 score. Fig. S6 shows that R^2 is 1.0 for all substrate lengths at polynomial degree 6.

The effectiveness of models trained using numerous combinations of polynomial degree and substrate thickness values is shown in Fig. S7(a) for TC R-30 and S7(b) for TC R-50 with the help of a heat map table representing R^2 score. Fig. S7 illustrates that R^2 score of 1.0 can be obtained for all substrate thickness values at polynomial degrees 6.

The effectiveness of models trained using numerous combinations of substrate width and polynomial degree values is shown in Fig. S8(a) for TC R-30 and S8(b) for TC R-50 with the help of a heat map table representing R^2 score. Fig. S8 illustrates that R^2 score of 1.0 can be obtained for all substrate width values at different polynomial degrees.

Scatterplots representing values of absorption predicted by PR models vs simulated values of absorption for angle=0 (TC R-30), graphene potential = 0.5 eV (TCR-30), resonator thickness = 0.2 µm (TCR-30), substrate length = 70 µm (TCR-30), substrate thickness = 0.6 µm (TC R-30), substrate width = 70 µm (TCR-30) are indicated in Fig. 7 (a-f) in that order. Diagonal placements of points in the graphs perceivably verify the prediction precision of PR models.

V. Conclusion

The biosensor is designed for detecting hemoglobin biomolecules with high sensitivity using polynomial regression models. Regression models are trained on six parameters (Angle of incidence, substrate length, substrate width, substrate thickness, graphene chemical potential, resonator thickness). The prediction accuracy close to 1.0 R^2 score is achieved for TCR-30 and TCR-50 using higher polynomial degrees. Geometrical parameters are analyzed which aims for achieving high sensitivity. The combination of gold metasurface based on graphene material is giving higher sensitivity for hemoglobin detection. The best sensitivity of 2000 nm/RIU is observed for proposed designs. The polynomial regression model can be used to predict different geometrical parameter values and can help in increasing the sensitivity by finding out the best suitable parameter. The proposed biosensor with its prediction capacity can be used in future biomedical devices.

References

[1] P. Mehrotra, "Biosensors and their applications - A review," *Journal of Oral Biology and Craniofacial Research*. 2016, doi: 10.1016/j.jobcr.2015.12.002.

[2] C. Liu, D. Jiang, G. Xiang, L. Liu, F. Liu, and X. Pu, "An electrochemical DNA biosensor for the detection of Mycobacterium tuberculosis, based on signal amplification of graphene and a gold nanoparticle-polyaniline nanocomposite," *Analyst*, 2014, doi: 10.1039/c4an00976b.

[3] N. Khansili, G. Rattu, and P. M. Krishna, "Label-free optical biosensors for food and biological sensor applications," *Sensors and Actuators, B: Chemical*, vol. 265. Elsevier B.V., pp. 35–49, Jul. 2018, doi: 10.1016/j.snb.2018.03.004.

[4] A. Singh, S. U. Rehman, S. Yongchareon, and P. H. J. Chong, "Sensor Technologies for Fall Detection Systems: A Review," *IEEE Sensors Journal*. 2020, doi: 10.1109/JSEN.2020.2976554.

[5] D. Gurkan and S. Gurkan, "Special section on sensor applications," *IEEE Transactions on Instrumentation and Measurement*. 2012, doi: 10.1109/TIM.2012.2208594.

[6] A. P. F. Turner, "Biosensors: Sense and sensibility," *Chem. Soc. Rev.*, 2013, doi: 10.1039/c3cs35528d.

[7] V. Singh, Juejun Hu, A. M. Agarwal, and L. C. Kimerling, "Integrated optical sensors," *IEEE Photonics J.*, 2012, doi: 10.1109/JPHOT.2012.2192721.

[8] S. K. Patel *et al.*, "Design of graphene metasurface based sensitive infrared biosensor," *Sensors Actuators, A Phys.*, vol. 301, 2020, doi: 10.1016/j.sna.2019.111767.

[9] P. Damborský, J. Švitel, and J. Katrlík, "Optical biosensors," *Essays Biochem.*, vol. 60, no. 1, pp. 91–100, Jun. 2016, doi: 10.1042/EBC20150010.

[10] M. Puentes, M. Schűßler, A. Penirschke, C. Damm, and R. Jakoby, "Metamaterials in microwave sensing applications," 2010, doi: 10.1109/ICSENS.2010.5690570.

[11] F. Monticone and A. Alù, "Metamaterials and plasmonics: From nanoparticles to nanoantenna arrays, metasurfaces, and metamaterials," *Chinese Physics B*. 2014, doi: 10.1088/1674-1056/23/4/047809.

[12] S. K. Patel, S. Charola, C. Jani, M. Ladumor, J. Parmar, and T. Guo, "Graphene-based highly efficient and broadband solar absorber," *Opt. Mater. (Amst).*, vol. 96, 2019, doi: 10.1016/j.optmat.2019.109330.

[13] S. K. Patel, J. Parmar, H. Trivedi, R. Zakaria, T. K. Nguyen, and V. Dhasarathan, "Highly Sensitive Graphene-Based Refractive Index Biosensor Using Gold Metasurface Array," *IEEE Photonics Technol. Lett.*, vol. 32, no. 12, pp. 681–684, 2020, doi: 10.1109/LPT.2020.2992085.

[14] O. Oshin, D. Kireev, H. Hlukhova, F. Idachaba, D. Akinwande, and A. Atayero, "Graphene-based biosensor for early detection of iron deficiency," *Sensors (Switzerland)*, 2020, doi: 10.3390/s20133688.

[15] N. Zheng, M. Aghadjani, K. Song, and P. Mazumder, "Metamaterial sensor platforms for Terahertz DNA sensing," 2013, doi: 10.1109/NANO.2013.6720831.

[16] Y. Lee, S. J. Kim, H. Park, and B. Lee, "Metamaterials and metasurfaces for sensor applications," *Sensors (Switzerland)*. 2017, doi: 10.3390/s17081726.

[17] T. H. Nguyen *et al.*, "Metamaterial-based perfect absorber: Polarization insensitivity and broadband," *Adv. Nat. Sci. Nanosci. Nanotechnol.*, vol. 5, no. 2, p. 25013, May 2014, doi: 10.1088/2043-6262/5/2/025013.

[18] J. Y. Rhee, Y. J. Yoo, K. W. Kim, Y. J. Kim, and Y. P. Lee, "Metamaterial-based perfect absorbers," *Journal of Electromagnetic Waves and Applications*, vol. 28, no. 13. Taylor and Francis Ltd., pp. 1541–1580, Sep. 2014, doi: 10.1080/09205071.2014.944273.

[19] S. Agarwal and Y. K. Prajapati, "Analysis of metamaterial-based absorber for thermo-photovoltaic cell applications," *IET Optoelectron.*, vol. 11, no. 5, pp. 208–212, Oct. 2017, doi: 10.1049/iet-opt.2016.0169.

[20] B.-X. Wang, G.-Z. Wang, L.-L. Wang, W.-Q. Huang, X. Zhai, and X.-F. Li, "Frequency Continuous Tunable Terahertz Metamaterial Absorber," *J. Light. Technol. Vol. 32, Issue 6, pp. 1183-1189*, vol. 32, no. 6, pp. 1183–1189, Mar. 2014.

[21] L. Feng, P. Huo, Y. Liang, and T. Xu, "Photonic Metamaterial Absorbers: Morphology Engineering and Interdisciplinary Applications," *Adv. Mater.*, vol. 32, no. 27, p. 1903787, Sep. 2019, doi: 10.1002/adma.201903787.

[22] H. Pakarzadeh, V. Sharif, D. Vigneswaran, and N. Ayyanar, "Graphene-assisted tunable D-shaped photonic crystal fiber sensor in the visible and IR regions," *J. Opt. Soc. Am. B*, vol. 39, no. 6, p. 1490, Jun. 2022, doi: 10.1364/JOSAB.450393.

[23] M. Askari, H. Pakarzadeh, and F. Shokrgozar, "High Q-factor terahertz metamaterial for superior refractive index sensing," *J. Opt. Soc. Am. B*, vol. 38, no. 12, p. 3929, 2021, doi: 10.1364/josab.438773.

[24] S. Barzegar-Parizi and A. Ebrahimi, "Ultrathin, polarization-insensitive multi-band absorbers based on graphene metasurface with THz sensing application," *J. Opt. Soc. Am. B*, vol. 37, no. 8, p. 2372, 2020, doi: 10.1364/josab.396266.

[25] J. Parmar, S. K. Patel, and V. Katkar, "Graphene-based metasurface solar absorber design with absorption prediction using machine learning," *Sci. Rep.*, vol. 12, no. 1, p. 2609, Dec. 2022, doi: 10.1038/s41598-022-06687-6.

[26] S. K. Patel, J. Surve, V. Katkar, and J. Parmar, "Machine learning assisted metamaterial-based reconfigurable antenna for low-cost portable electronic devices," *Sci. Rep.*, vol. 12, no. 1, p. 12354, Dec. 2022, doi: 10.1038/s41598-022-16678-2.

[27] S. K. Patel, J. Surve, V. Katkar, and J. Parmar, "Optimization of Metamaterial-Based Solar Energy Absorber for Enhancing Solar Thermal Energy Conversion Using Artificial Intelligence," *Adv. Theory Simulations*, p. 2200139, May 2022, doi: 10.1002/adts.202200139.

[28] S. K. Patel *et al.*, "Graphene-Based Highly Sensitive Refractive Index Biosensors Using C-Shaped Metasurface," *IEEE Sens. J.*, vol. 20, no. 12, pp. 6359–6366, 2020, doi: 10.1109/JSEN.2020.2976571.

[29] P. K. Jain, K. S. Lee, I. H. El-Sayed, and M. A. El-Sayed, "Calculated absorption and scattering properties of gold nanoparticles of different size, shape, and composition: Applications in biological imaging and biomedicine," *J. Phys. Chem. B*, vol. 110, no. 14, pp. 7238–7248, 2006, doi: 10.1021/jp057170o.

[30] S. Zhang *et al.*, "Metasurfaces for biomedical applications: Imaging and sensing from a nanophotonics perspective," *Nanophotonics*, vol. 10, no. 1, pp. 259–293, 2021, doi: 10.1515/nanoph-2020-0373.

[31] J. Yoon, H. Y. Cho, M. Shin, H. K. Choi, T. Lee, and J. W. Choi, "Flexible electrochemical biosensors for healthcare monitoring," *Journal of Materials Chemistry B*, vol. 8, no. 33. pp. 7303–7318, 2020, doi: 10.1039/d0tb01325k.

[32] A. K. Ajad, M. J. Islam, M. R. Kaysir, and J. Atai, "Highly sensitive bio sensor based on WGM ring resonator for hemoglobin detection in blood samples," *Optik (Stuttg).*, 2021, doi: 10.1016/j.ijleo.2020.166009.

[33] S. Sahu, J. Ali, P. P. Yupapin, and G. Singh, "Porous Silicon Based Bragg-Grating Resonator for Refractive Index Biosensor," *Photonic Sensors*, vol. 8, no. 3, pp. 248–254, 2018, doi: 10.1007/s13320-018-0459-z.

[34] S. K. Patel *et al.*, “Encoding and tuning of THz metasurface-based refractive index sensor with behavior prediction using XGBoost Regressor,” *IEEE Access*, pp. 1–1, 2022, doi: 10.1109/ACCESS.2022.3154386.

[35] Z. Wang, Z. Geng, and W. Fang, “Exploring performance of THz metamaterial biosensor based on flexible thin-film,” *Opt. Express*, vol. 28, no. 18, p. 26370, 2020, doi: 10.1364/oe.402222.

[36] S. K. Patel, J. Parmar, V. Sorathiya, R. Zakaria, V. Dhasarathan, and T. K. Nguyen, “Graphene-Based Plasmonic Absorber For Biosensing Applications Using Gold Split Ring Resonator Metasurfaces,” *J. Light. Technol.*, 2021, doi: 10.1109/JLT.2021.3069758.

[37] Z. Wei *et al.*, “Analogue Electromagnetically Induced Transparency Based on Low-loss Metamaterial and its Application in Nanosensor and Slow-light Device,” *Plasmonics*, vol. 12, no. 3, pp. 641–647, 2017, doi: 10.1007/s11468-016-0309-z.

[38] X. J. He, L. Wang, J. M. Wang, X. H. Tian, J. X. Jiang, and Z. X. Geng, “Electromagnetically induced transparency in planar complementary metamaterial for refractive index sensing applications,” *J. Phys. D. Appl. Phys.*, vol. 46, no. 36, 2013, doi: 10.1088/0022-3727/46/36/365302.

[39] M. Wan, S. Yuan, K. Dai, Y. Song, and F. Zhou, “Electromagnetically induced transparency in a planar complementary metamaterial and its sensing performance,” *Optik (Stuttg).*, vol. 126, no. 5, pp. 541–544, 2015, doi: 10.1016/j.ijleo.2015.01.006.

[40] G. An *et al.*, “Ultra-stable D-shaped Optical Fiber Refractive Index Sensor with Graphene-Gold Deposited Platform,” *Plasmonics*, vol. 14, no. 1, pp. 155–163, 2019, doi: 10.1007/s11468-018-0788-1.

[41] G. J. Székely and M. L. Rizzo, “Brownian distance covariance,” *Ann. Appl. Stat.*, vol. 3, no. 4, pp. 1236–1265, 2009, doi: 10.1214/09-AOAS312.

[42] E. Ostertagová, “Modelling using polynomial regression,” in *Procedia Engineering*, 2012, vol. 48, pp. 500–506, doi: 10.1016/j.proeng.2012.09.545.